June 2007

Realization of Receptive Fields with Excitatory and Inhibitory Responses on Equilibrium-State Luminescence of Electron Trapping Material Thin Film

Ramin Pashaie
University of Pennsylvania, raminp@seas.upenn.edu

Nabil H. Farhat
University of Pennsylvania, farhat@seas.upenn.edu

Realization of Receptive Fields with Excitatory and Inhibitory Responses on Equilibrium-State Luminescence of Electron Trapping Material Thin Film

Abstract
Our theoretical modelings and experimental observations illustrate that the equilibrium-state luminescence of electron-trapping materials (ETMs) can be controlled to produce either excitatory or inhibitory responses to the same optical stimulus. Because of this property, ETMs have a unique potential in optical realization of neurobiologically based parallel computations. As a classic example, we have controlled the equilibrium-state luminescence of a thin film of this stimulable storage phosphor to make it behave similarly to the receptive fields of sensory neurons in the mammalian visual system, which are responsible for early visual processing.

Keywords
information processing, optical data processing, optical neural systems

Realization of receptive fields with excitatory and inhibitory responses on equilibrium-state luminescence of electron trapping material

Ramin Pashaie* and Nabil H. Farhat

Department of Electrical and Systems Engineering, University of Pennsylvania, 220 South 33rd Street, Philadelphia, Pennsylvania 19104, USA

**Corresponding author: raminp@seas.upenn.edu*

Received January 17, 2007; revised March 8, 2007; accepted March 20, 2007; posted March 28, 2007 (Doc. ID 78555); published May 7, 2007

Our theoretical modelings and experimental observations illustrate that the equilibrium-state luminescence of electron-trapping materials (ETMs) can be controlled to produce either excitatory or inhibitory responses to the same optical stimulus. Because of this property, ETMs have a unique potential in optical realization of neurobiologically based parallel computations. As a classic example, we have controlled the equilibrium-state luminescence of a thin film of this stimulable storage phosphor to make it behave similarly to the receptive fields of sensory neurons in the mammalian visual system, which are responsible for early visual processing.

OCIS codes: 200.4560, 200.4700, 200.3050, 200.4560.

Image processing in a number of mammals, including humans, begins with early visual processing in the retina and the lateral geniculate nucleus (LGN) and continues in the primary visual cortex (area 17) [1,2]. During highly parallel computational schemes, many features of the image (e.g., contrast, edges, spatial frequencies and direction of motion) are detected by real-time spatial filtering and differential operations. Such computational power stems from the physical shape of neuron's receptive fields (RFs) with excitatory and inhibitory responses [3]. Isotropic RFs of neurons in the retina and the LGN and the orientation-selective RFs of neurons in the primary visual cortex are depicted in Figs. 1(a)–1(d) [1]. The presence of stimuli in the dark area of each RF hyperpolarizes the corresponding neuron and reduces its activity. In contrast, a stimulus in the bright area depolarizes the neuron and increases neuronal activity. Areas with little effects are shown in medium gray. By comparing the firing rate of the center to the surround, the neuron can encode the contrast information of the optical stimulation. Spatial frequency of the image can be extracted from the firing rate of the cells of different RF sizes. Small RFs are sensitive to high spatial frequencies and fine details of image, whereas larger RFs are sensitive to low spatial frequencies. Direction of movement can be detected by neurons that have spatial–temporal RFs. Successive snapshots of such spatial–temporal RFs are shown in Fig. 1(e) [1].

Previous researchers have used different enabling technologies to realize this neurobiologically based parallel computation. Mead and Mahowald's attempts resulted in a VLSI artificial retina [4]. Armitage and Thackara implemented an optical system by combining photoconductive material and liquid crystal [5]. Takei employed the inherent ability of bacteriorhodopsin molecules to emulate inhibition and excitation in neural computation [6]. Recently, Gruev presented a VLSI pseudo-general image processor that is capable of applying different spatial–temporal filters, including Gabor filters, to a captured image during readout [7].

In this paper a particular type of stimulable storage phosphor known as electron-trapping material (ETM) is studied for optical realization of a similar computational mechanism. We illustrate that the equilibrium-state luminescence of ETMs can be designed to exhibit controllable excitatory and inhibitory behaviors. By combining this property with high-resolution capabilities of ETM and state of the art spatial light modulators (SLMs), dense arrays of static and spatial–temporal RFs can be implemented in an ETM thin film.

ETMs are alkaline-earth sulfides doped with rare-earth luminescence centers [8]. Because of many attractive properties, including high resolution and wavelength diversity, this material has great potential for technical applications such as three-dimensional memories, infrared sensors, and display devices. Also ETMs have been employed in the struc-

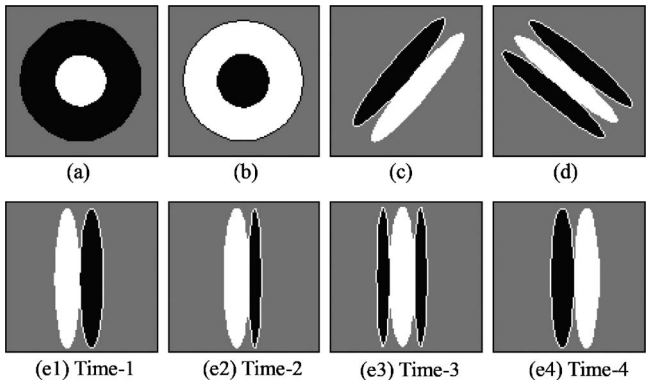

Fig. 1. Static and spatial–temporal RFs of biological neurons: (a) ON cell in retina and LGN, (b) OFF cell in retina and LGN, (c) orientation-selective RF in primary visual cortex sensitive to 45° edge with dark in the upper left and light in the lower right, (d) orientation-selective RF in primary visual cortex sensitive to 135° edge sensitive to a white line on a dark background, (e) spatial–temporal RFs at Time-1–Time-4 [1].

0146-9592/07/111501-3/$15.00

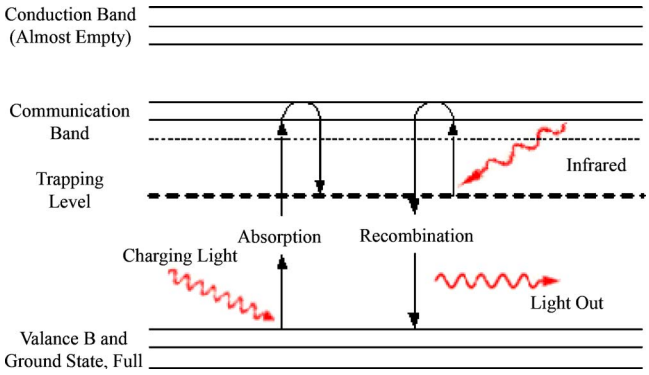

Fig. 2. (Color online) Atomic band structure of ETM.

ture of computational machines and biological models [9–11]. The atomic band structure and the optical mechanism of ETM are illustrated in Fig. 2. Rare-earth-doped elements add a trap energy level within the host bandgap. Interaction of electrons and blue photons (wavelength around 450 nm) can transfer sufficient energy to valance band electrons and excite them to higher energy levels. Some of these electrons tunnel to the trap energy level and become trapped electrons. Blue photons also have enough energy to detrap some of the trapped electrons. Nevertheless, in an environment without optical stimulations, trapped electrons remain in the trap energy levels forever. On the other hand, exposing ETM to near-infrared (NIR) light (wavelength around 1310 nm) can excite some of the trapped electrons and kick them out of the trap level. These electrons release their extra energy as orange photons (wavelength around 650 nm) when they return to the host valance band. In this process the intensity of orange luminescence is proportional to the intensity of optical stimulations and the wavelength-dependent parameters of the material. Under simultaneous blue light and NIR illumination, the intensity of orange luminescence (after a short transient) merges to a constant value called the equilibrium-state luminescence of ETM. We have recently shown that the equilibrium-state luminescence of ETM can be formulated by the following equations [12]:

$$\frac{4\xi}{\eta} I_B \sinh^2\left(\frac{n_s - n}{2\xi I_B}\right) = \frac{4\xi'}{\eta'} I_{NIR} \sinh^2\left(\frac{n}{2\xi' I_{NIR}}\right), \quad (1)$$

$$I_O = \alpha n(t) I_B + \beta n(t) I_{NIR}. \quad (2)$$

In these equations I_B and I_{NIR} represent the intensity of blue and NIR light, respectively. I_O is the intensity of orange luminescence; ξ, η, ξ', η', α, and β are the wavelength-dependent parameters of the material; $n(t)$ is the density of the trapped electrons; and n_s is the saturation level of $n(t)$. For any specified values of the blue and NIR irradiance, the intensity of the corresponding orange luminescence can be calculated by the equations. Figure 3 is an equilibrium-state plane showing intensity contours of constant orange luminescence plotted as a function of the intensity of the blue light and the NIR irradiance. The numbers on the contours are the output voltage of the photodetector that measured the intensity of orange luminescence. The subtle point of this diagram can be highlighted by investigation of four sample points, S, P, Q, and R. Despite different NIR and blue exposures on points S and Q, these two points are on the same contour. Consequently, the intensity of orange luminescence at points S and Q is equal. This can be justified intuitively by considering the fact that the intensity of orange luminescence is proportional to the rate of detrapping. Meanwhile, the rate of detrapping is proportional to the probability of interaction between NIR photons and trapped electrons. In the diagram, lower NIR exposure at point Q compared with point S is compensated by higher blue illumination, which increases the population of trapped electrons and the probability of interaction. Blue exposure at the points P, Q, and R is equal; however, NIR irradiance is more at P and less at R compared with NIR irradiance at Q. Higher NIR exposure at P increases the rate of detrapping and the corresponding orange luminescence compared with Q. Conversely, orange luminescence at R is less than Q as a result of lower NIR illumination.

Now consider the case where two light sources are linearly coupled. In this case, based on the parameters of linear coupling, only intensities of orange luminescence along a line are accessible in the equilibrium-state plane. For linear coupling along the line SP (from S to P) the intensity of orange luminescence increases monotonically, which is an excitatory reaction to the extra blue illumination. Conversely, from point S to R along the line SR, the intensity of orange luminescence decreases and the reaction is inhibitory. Along SQ the level of orange luminescence does not change considerably, similar to the gray areas in Fig. 1. If ETM is biased at S (the resting point) and external stimulations are applied by extra blue exposure, then depending on the coupling parameters, the behavior of ETM can be either excitatory or inhibitory. Hence, the type and the intensity of ETM's reaction to an external excitation depends on the coupling parameters.

To verify the above observation an experiment is organized. Figure 4 displays the schematic of the optical setup. An ETM panel (25 mm × 25 mm thin film of $SrSEu^{2+}:Sm^{3+}$ coated on a quartz substrate [13]) is

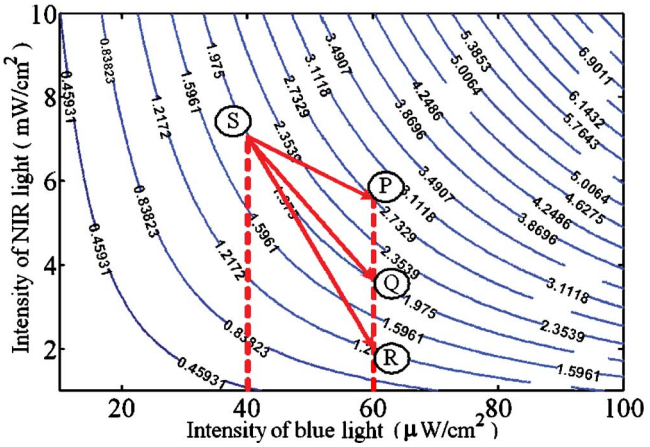

Fig. 3. (Color online) Equilibrium-state plane of ETM.

exposed to the combined beam of two pairs of linearly coupled light sources, (B1, NIR1) and (B2, NIR2). (B1, NIR1) and (B2, NIR2) are coupled with suitable coupling parameters to produce excitatory and inhibitory regions of a RF, respectively. B1 and B2 are bright blue LEDs, and NIR1 and NIR2 are Exalos 1310 nm, 20 mW superluminescent laser diodes. Two masks, M1 and M2, adjust the shape and the size of each region. In this experiment, areas of both ON and OFF regions are fixed to 3 mm^2. An avalanche photodetector (Hamamatsu APD module CA4777-01) detects orange luminescence through an orange optical filter (Semrock LP01-633Rs-25). External stimulation is directed to B1 or B2 by two switches, S1 and S2. To produce the resting point both light source couples illuminate ETM with $I_B=40\ \mu W/cm^2$ and $I_{NIR}=10\ mW/cm^2$ for which ADP generates 3.5 V in the equilibrium state. The equilibrium happens approximately after 100 ms. During the first experiment, S1 is closed and S2 is open to stimulate the ON region of the RF and the intensity of the blue irradiance is swept up to $I_B=60\ \mu W/cm^2$. During this experiment the equilibrium-state output voltages of the APD monotonically increases up to 4.9 V (Fig. 5). In the second experiment, stimulations are applied to the OFF region by closing S2 and opening S1. This time, increasing the blue exposure reduces the orange luminescence, and at $I_B=60\ \mu W/cm^2$ the APD's output voltage drops to 2.3 V. By choosing suitable coupling parameters one can make each region more or less sensitive to the optical stimulation.

Our experimental results convincingly show the potential of ETM to produce controllable excitatory and inhibitory reactions. Dense arrays of RFs with a variety of shapes and dimensions can be realized in ETM thin film by illuminating the ETM panel with two SLMs, such as Texas Instruments Digital Micromirror Devices. In such an optical setup one SLM modulates the intensity of NIR illumination when the other SLM provides the modulated blue light exposure. The pixels of the two SLMs are linearly coupled (via driving electronics) with suitable coupling parameters to generate variety of different reactions to the same stimulus. By changing the modulation and the coupling parameters of the pixels, such

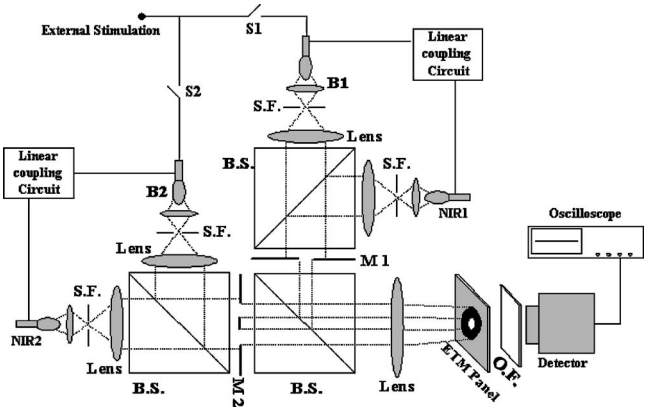

Fig. 4. Schematic of the optical setup: B.S., beam splitter; S.F., spatial filter, O.F., optical filter. Other abbreviations defined in text.

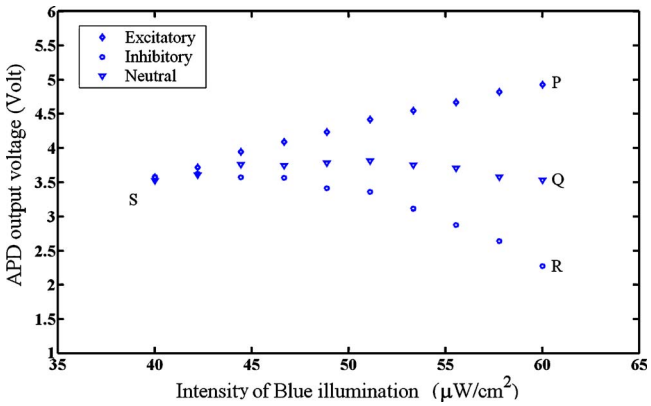

Fig. 5. (Color online) Experimental results. When external stimulus is applied to the ON (OFF) region, the level of orange luminescence changes from S to P (R). Along SQ, stimulus is applied to the ON region, and (B1, NIR1) are coupled so as to be less sensitive to external excitation.

an optical setup would be capable of dynamically reprogramming the ETM for the generation of different RFs including spatial–temporal RFs. Despite the flexibility of this approach, the only drawback is the fact that all the interesting behaviors happen in the equilibrium state. So after illumination one should wait until the transient response is passed. This delay time reduces the speed of the parallel computations. Fortunately, because of the electronic nature of all the processes, speed of computations can be improved by using ETMs with a faster response.

This research was supported in part by Army Research Office MURI grant prime DAAD 19-01-0603 via Georgia Institute of Technology subcontract E-18-677-64 and in part by Office of Naval Research grant N00014-94-1-0931.

References

1. R. Miikkulainen, J. A. Bednar, Y. Choe, and J. Sirosh, *Computational Maps in the Visual Cortex* (Springer, 2005).
2. M. F. Bear, B. W. Connors, and M. A. Paradiso, *Neuroscience Exploring the Brain* (Lippincott, 2001).
3. R. W. Rodieck and J. Stone, J. Neurophysiol. **28**, 833 (1965).
4. C. A. Mead and M. A. Mahowald, Neural Networks **1**, 91 (1988).
5. D. Armitage and J. I. Thackara, Appl. Opt. **28**, 219 (1989).
6. H. Takei, A. Lewis, Z. Chen, and L. Nebenzahl, Appl. Opt. **30**, 500 (1991).
7. V. Gruev and R. Etienne-Commings, IEEE Trans. Circuits Syst., II: Analog Digital Signal Process. **49**, 233 (2002).
8. S. Jutamulia, G. M. Storti, J. Lindmayer, and W. Seiderman, Appl. Opt. **30**, 2879 (1991).
9. S. Jutamuli, G. Stori, J. Lindmayer, and W. Seiderman, Appl. Opt. **32**, 743 (1993).
10. Z. Wen, A. Baek, and N. Farhat, Opt. Lett. **20**, 614 (1995).
11. Z. Wen and N. Farhat, Appl. Opt. **34**, 5188 (1995).
12. R. Pashaie and N. Farhat, "Dynamics of electron-trapping materials under blue light and near-infrared exposure: a new model," submitted to JOSA B.
13. The ETM sample for this research was furnished by Quantex Inc., Rockville, Maryland.